Slow viscous motion of a solid particle in a spherical cavity

A. Sellier[1]

Abstract: The slow viscous and either imposed or gravity-driven migration of a solid arbitrarily-shaped particle suspended in a Newtonian liquid bounded by a spherical cavity is calculated using two different boundary element approaches. Each advocated method appeals to a few boundary-integral equations and, by contrast with previous works, also holds for non-spherical particles. The first procedure puts usual free-space Stokeslets on both the cavity and particle surfaces whilst the second one solely spreads specific Stokeslets obtained elsewhere in Oseen (1927) on the particle's boundary. Each approach receives a numerical implementation which is found to be in excellent agreement with accurate results available for spherical particles. The computations for spheroidal or ellipsoidal particles, here accurately achieved at a very reasonable cpu time cost using the second technique, reveal that the particle settling migration deeply depends upon the gravity and upon both its shape and location inside the cavity.

Keyword: Stokes flow, wall-particle interactions, spherical cavity, sedimentation, Green tensor, boundary-integral equations.

1 Introduction

Many applications involve suspensions of solid particles immersed in a Newtonian liquid with uniform viscosity μ and density ρ. For dilute suspensions particles ignore each other, at least at the very first order, and it therefore becomes of prime interest to determine the net hydrodynamic force $\mathbf{F}_h$ and torque $\mathbf{T}_h$ exerted on a solid particle translating and rotating in a quiescent liquid at prescribed velocities $\mathbf{U}$ (the velocity of a point O' attached to the particle) and $\mathbf{W}$, respectively. In

[1] LadHyX, Ecole Polytechnique, FRANCE

practice, the Reynolds number $\mathrm{Re} = \rho V a / \mu$, with a and V the particle length and velocity scales, is small so that inertial effects are negligible and the liquid experiences a quasi-static Stokes flow. In the past decades the vectors $\mathbf{F}_h$ and $\mathbf{T}_h$ have been obtained within this widely-employed framework using analytical or numerical treatments for either spherical or non-spherical particles moving in unbounded or bounded liquid domains. When the fluid is not bounded the only analytical results (for three-dimensional particles, i. e. not for thin ones such as a disk for instance) have been obtained (see Happel and Brenner (1973)) for ellipsoidal particles only. For a sphere with radius a and center O' the quite simple and widely-employed results read

$$\mathbf{F}_h = -6\pi\mu a\mathbf{U}, \quad \mathbf{T}_h = -8\pi\mu a^3\mathbf{W}. \qquad (1)$$

Accordingly, a sphere with radius a and uniform density ρ_s immersed in an unbounded fluid settles under the uniform gravity field $\mathbf{g}$ at the following translational velocity $\mathbf{U}_s$ and angular velocity $\mathbf{W}_s$

$$\mathbf{U}_s = 2(\rho_s - \rho)a^2\mathbf{g}/(9\mu), \quad \mathbf{W}_s = \mathbf{0}. \qquad (2)$$

For arbitrarily-shaped particles $\mathbf{F}_h$ and $\mathbf{T}_h$ in general depend by contrast upon both $\mathbf{U}$ and $\mathbf{W}$ and can be numerically evaluated by appealing to the so-called boundary element approach and its numerical implementation (see Pozrikidis (1992)). Because the results prevailing for an unbounded fluid may be significantly affected close to boundaries many several works also investigated to which extent $\mathbf{F}_h, \mathbf{T}_h$ and the resulting particle settling migration depend upon particle-wall interactions. In this direction one should first mention the case of a plane, solid and motionless boundary. Such circumstances have been analytically and extensively addressed for a spherical particle by resorting to the bipolar coordinates by several authors (see, among others, Brenner (1961); Goldman, Cox, and Brenner (1967a);

Dean and O'Neill (1963); O'Neill (1964, 1967); O'Neill and Stewartson (1967)). The case of a sphere freely suspended or kept at rest near the wall in different ambient Stokes flows was treated, again using this method, by Goldman, Cox, and Brenner (1967b), Chaoui and Feuillebois (2003), Pasol, Chaoui, Yahiaoui, and Feuillebois (2005) and Pasol, Sellier, and Feuillebois (2006) whereas a different and collocation approach has been worked out in Hsu and Ganatos (1989, 1994) for a non-spherical particle in a quiescent liquid. It is also worth noting the powerful and different method of multipole images introduced and applied for a single sphere in Cichocki and Jones (1998) and also further successfully worked out for a $N - sphere$ cluster immersed in a Stokes flow in the vicinity of a plane hard wall or free surface in Cichocki, Jones, Kutteh, and Wajnryb (2000). The case of two parallel, plane, solid and motionless boundaries also received attention in the past decades with results provided for a sphere by Ganatos, Peffer, and Weibaum (1980a,b) using a collocation approach and by Jones (2004) introducing a new and specific Green tensor. Finally, Staben, Zinchenko, and Davis (2003) and Pasol and Sellier (2006) were also able to cope with non-spherical particles by means of different boundary-integral approaches based on the use of a specific Green tensor. Adding more boundaries further suggests to confine the liquid by a cavity. In such circumstances, very strong particle-boundary effects are likely to take place as revealed by several results available for a solid sphere moving in a liquid bounded by a spherical cavity. For instance, the net force $\mathbf{F}_h$ exerted on and the flow about a translating sphere (i. e. for $\mathbf{W} = \mathbf{0}$) located at the spherical cavity center have been obtained using a stream function in Cunningham (1910); Williams (1915). The more tricky case of a sphere not located at the spherical cavity center was solved using bipolar coordinates by Jeffery (1915); Stimson and Jeffery (1926) for the axisymmetrical migration and by O'Neill and Majumdar (1970a,b) for the asymmetrical motion. Such nice analytical techniques have been recently revisited in Jones (2008) where a very accurate implementation is achieved and an omission in O'Neill and Majumdar (1970a) is cor-

rected. Unfortunately but not surprisingly, the fruitful use of bipolar coordinates prevents each previous work to cope with the challenging case of a non-spherical particle in a spherical cavity. The present work therefore advocates a boundary-integral approach which makes it possible to accurately compute at a reasonable cpu time cost the net force and torque exerted on a non-spherical particle experiencing a precribed rigid-body motion in a liquid bounded by a spherical cavity and its resulting gravity-driven migration.

The paper is organized as follows. The relevant assumptions and the governing equations are presented in §2 whereas two suitable boundary-integral approaches for a rigid-body motion of a particle of arbitrary shape and a specific Green tensor established by Oseen (1927) are introduced in §3. It is shown in §4 how to obtain the particle settling migration and, if needed, the liquid flow about it. The numerical implementation is described and each proposed boundary-integral method is then numerically tested against available analytical results for a spherical particle in §5. New results for spheroidal and ellipsoidal particles are presented and discussed in §6 and a few concluding remarks close the paper in §7.

2 Governing problem

We consider, as illustrated in Fig. 1, a solid and arbitrarily-shaped particle $\mathscr{P}$ with smooth enough boundary S, uniform density ρ_s and volume $\mathscr{V}$ subject to a uniform gravity field $\mathbf{g}$ and immersed in a Newtonian liquid with uniform density ρ and viscosity μ bounded by a solid sphere with center O, radius R and surface Σ. Henceforth, we adopt Cartesian coordinates (O, x_1, x_2, x_3) attached to the Laboratory and for any point M in the spherical cavity or on its boundary Σ we set $\mathbf{x} = \mathbf{OM}$ with $r = |\mathbf{x}| \leq R$ and $x_i = \mathbf{x}.\mathbf{e}_i$ for $i = 1, 2, 3$. The solid cavity is furthermore assumed to rotate parallel to the vector $\mathbf{e}$ at the sufficiently small angular velocity $w_c \mathbf{e}$ such that $\mathrm{Re}_{w_c} = \rho |w_c| R^2 / \mu \ll 1$ whereas the particle experiences a rigid-body motion characterized by the translational velocity $\mathbf{U}$, here selected as the velocity of the particle center of mass O', and the angular velocity $\mathbf{W}$. Since in absence of particle
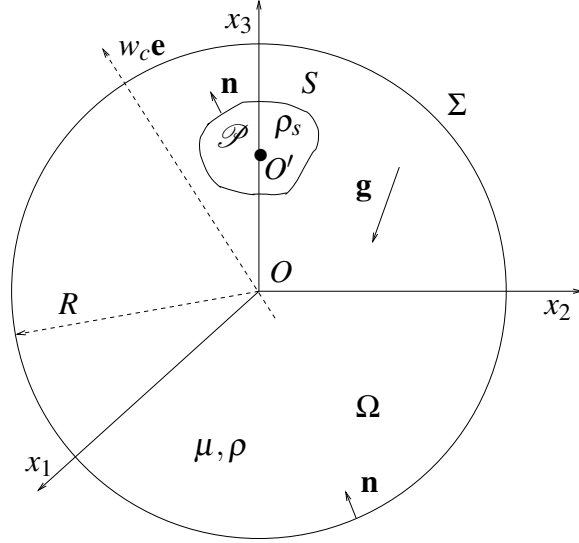
Figure 1: A solid particle $\mathscr{P}$ with center of mass O' immersed in a Newtonian liquid bounded by a solid and possibly-rotating spherical sphere.

the fluid has pressure $p_{ext} = \rho \mathbf{g}.\mathbf{x}$ and velocity $\mathbf{u}_{ext} = w_c \mathbf{e} \wedge \mathbf{x}$ we thus denote the disturbed velocity and pressure fields in the liquid by $\mathbf{u}_t = \mathbf{u} + w_c \mathbf{e} \wedge \mathbf{x}$ and $p_t = p + \rho \mathbf{g}.\mathbf{x}$, respectively. Observing that $\mathbf{u}_{ext}$ is a Stokes flow and assuming, if $\mathscr{P}$ has length scale a and $\mathbf{u}$ typical magnitude V, that $\mathrm{Re} = \rho V a / \mu \ll 1$ makes it possible to neglect inertial effects. Accordingly, the disturbances $\mathbf{u}$ and p are governed by the following quasi-static Stokes equations and velocity boundary conditions

$$\mu \nabla^2 \mathbf{u} = \nabla p \ \text{ and } \ \nabla.\mathbf{u} = 0 \ \text{ in } \ \Omega, \qquad (3)$$

$$\mathbf{u} = \mathbf{U} + \mathbf{W} \wedge \mathbf{x}' - w_c \mathbf{e} \wedge \mathbf{x} \ \text{ on } \ S, \qquad (4)$$

$$\mathbf{u} = \mathbf{0} \text{ on } \Sigma \qquad (5)$$

where Ω is the liquid domain and $\mathbf{x}' = \mathbf{O'M}$. If $\mathbf{n}$ designates the unit outward normal on $S \cup \Sigma$ directed into the liquid, the flow $(\mathbf{u}, p)$ with stress tensor $\boldsymbol{\sigma}$ exerts on the particle a net hydrodynamic force $\mathbf{F}_h$ and a net hydrodynamic torque $\mathbf{T}_h$ (about O') given by

$$\mathbf{F}_h = \int_S \boldsymbol{\sigma}.\mathbf{n} dS, \ \ \mathbf{T}_h = \int_S \mathbf{O'M} \wedge \boldsymbol{\sigma}.\mathbf{n} dS. \qquad (6)$$

At that stage it is worth pointing out that $\mathbf{F}_h$ and $\mathbf{T}_h$ are the net force and torque applied on the par-

ticle by the disturbed flow $(\mathbf{u}_{ext} + \mathbf{u}, p_{ext} + p)$ because the rigid-body external flow $(\mathbf{u}_{ext}, p_{ext})$ applies zero net force and torque on the particle. For a prescribed geometry (i. e. for given value of the cavity radius R and particle's shape and location) both the vectors $\mathbf{F}_h$ and torque $\mathbf{T}_h$ depend upon the setting $(w_c \mathbf{e}, \mathbf{g})$ and the rigid-body motion $(\mathbf{U}, \mathbf{W})$. In practice, two basic and different circumstances arise:

(i) One looks at the net hydrodynamic force and torque experienced by a particle with imposed translational and angular velocities for a possibly rotating cavity. This issue, reducing to the determination of $\mathbf{F}_h$ and $\mathbf{T}_h$ for $(\mathbf{u}, p)$ governed by (3)-(5), is theoretically handled in §3.

(ii) One looks at the particle's rigid-body $(\mathbf{U}, \mathbf{W})$ for a given gravity field $\mathbf{g}$ and/or a prescribed cavity rotation $w_c \mathbf{e}$. Neglecting the particle inertia this is achieved by requiring zero force and torque on the particle. Since this latter has a uniform density ρ_s one has therefore to solve the problem (3)-(5) in conjunction with the additional relations

$$\int_S \boldsymbol{\sigma}.\mathbf{n} dS = (\rho - \rho_s)\mathscr{V}\mathbf{g}, \ \ \int_S \mathbf{x}' \wedge \boldsymbol{\sigma}.\mathbf{n} dS = \mathbf{0}. \qquad (7)$$

As explained in §4, it is actually possible to also treat this case by exploiting the material developed in §3.

3 Rigid-body motion of a particle

Within this section the particle experiences a prescribed rigid-body motion $(\mathbf{U}, \mathbf{W})$ in a rotating cavity. Two approaches, valid whatever the particle's shape and consisting of the treatment of six boundary-integral equations on a surface $\mathscr{S}$, are proposed. The first one is by essence also able to cope with arbitrarily-shaped cavities but involves the entire surface $\mathscr{S} = S \cup \Sigma$ whereas the second one, restricted to spherical cavities, appeals to a specific Green tensor and thereby only involves the particle's surface with this time $\mathscr{S} = S$.

3.1 *Relevant surface quantities*

By virtue of (4) note that $\mathbf{u} = \mathbf{U}' + \mathbf{W}' \wedge \mathbf{x}'$ on S with $\mathbf{U}' = \mathbf{U} + w_c \mathbf{OO'} \wedge \mathbf{e}$ and $\mathbf{W}' = \mathbf{W} - w_c \mathbf{e}$.

Accordingly, it is sufficient by linearity to restrict in this section the attention to six auxiliary Stokes flows $(\mathbf{u}_T^{(i)}, p_T^{(i)})$ and $(\mathbf{u}_R^{(i)}, p_R^{(i)})$ for $i = 1, 2, 3$ which obey (3) and, for $L = T, R$, the specific boundary conditions

$$\mathbf{u}_T^{(i)} = \mathbf{e}_i \text{ and } \mathbf{u}_R^{(i)} = \mathbf{e}_i \wedge \mathbf{x}' \text{ on } S, \ \mathbf{u}_L^{(i)} = \mathbf{0} \text{ on } \Sigma. \tag{8}$$

The flow $(\mathbf{u}_L^{(i)}, p_L^{(i)})$ with stress tensor $\sigma_L^{(i)}$ exerts on the particle's surface S the traction $\mathbf{f}_L^{(i)} = \sigma_L^{(i)}.\mathbf{n}$ and $\mathbf{f}_T^{(i)}$ or $\mathbf{f}_R^{(i)}$ accordingly designates the surface force which arises on S if the particle translates or rotates parallel to $\mathbf{e}_i$, respectively. These vectors readily produce on the particule the following net hydrodynamic force $-\mathbf{A}_L^{(i)}$ and torque $-\mathbf{B}_L^{(i)}$ such that

$$\mathbf{A}_L^{(i)} = -\int_S \mathbf{f}_L^{(i)} dS, \ \mathbf{B}_L^{(i)} = -\int_S \mathbf{x}' \wedge \mathbf{f}_L^{(i)} dS. \tag{9}$$

In summary, the problem reduces to the determination of the relevant surface quantities $\mathbf{f}_T^{(i)}$ and $\mathbf{f}_R^{(i)}$.

3.2 Velocity integral representation and related boundary-integral equations

We introduce for a so-called pole $\mathbf{y}$ in $\mathscr{D} = \Omega \cup \mathscr{P}$ and $j = 1, 2, 3$ three Stokes flows $(\mathbf{v}^{(j)}, p^{(j)})$, with stress tensor $\sigma^{(j)}$, such that

$$\mu \nabla^2 \mathbf{v}^{(j)} = \nabla p^{(j)} - \delta_{3d}(\mathbf{x} - \mathbf{y})\mathbf{e}_j, \ \nabla.\mathbf{v}^{(j)} = 0 \text{ in } \mathscr{D} \tag{10}$$

with $\delta_{3d}(\mathbf{x} - \mathbf{y}) = \delta_d(x_1 - y_1)\delta_d(x_2 - y_2)\delta_d(x_3 - y_3)$ if $y_i = \mathbf{y}.\mathbf{e}_i$ and δ_d designates the Dirac pseudo-function. Clearly, the above velocity fields $\mathbf{v}^{(j)}(\mathbf{x}, \mathbf{y})$ and therefore the resulting Green tensor $\mathbf{G}$ with Cartesian components $G_{kj}(\mathbf{x}, \mathbf{y}) = \mathbf{v}^{(j)}(\mathbf{x}, \mathbf{y}).\mathbf{e}_k$ are not unique since (10) is not supplemented with velocity boundary conditions on the boundary Σ of $\mathscr{D}$. A simple and widely-employed Green tensor is the free-space Oseen-Burgers tensor $\mathbf{G}^\infty$ with Cartesian coordinates G_{kj}^∞ such that

$$8\pi\mu G_{kj}^\infty(\mathbf{x}, \mathbf{y}) = \frac{\delta_{kj}}{|\mathbf{x} - \mathbf{y}|} + \frac{[(\mathbf{x} - \mathbf{y}).\mathbf{e}_j][(\mathbf{x} - \mathbf{y}).\mathbf{e}_k]}{|\mathbf{x} - \mathbf{y}|^3}$$

$$\tag{11}$$

where δ denotes the Kronecker delta symbol.

We henceforth adopt the usual tensor summation convention and consider a Stokes flow $(\mathbf{u}, p)$ obeying (3) with stress tensor σ and surface traction $\mathbf{f} = \sigma.\mathbf{n} = f_k \mathbf{e}_k$ on S. The velocity $\mathbf{u} = u_j \mathbf{e}_j$ then admits in the entire liquid domain the representation (see Pozrikidis (1992))

$$u_j(\mathbf{x}) = -\int_{S \cup \Sigma} f_k(\mathbf{y}) G_{kj}(\mathbf{y}, \mathbf{x}) dS(\mathbf{y})$$
$$+ \int_{S \cup \Sigma} \mathbf{u}(\mathbf{y}). \sigma^{(j)}(\mathbf{x}, \mathbf{y}).\mathbf{n}(\mathbf{y}) dS(\mathbf{y}) \text{ for } \mathbf{x} \text{ in } \Omega.$$

$$\tag{12}$$

As detailed in Pozrikidis (1992) the Green tensor satisfies the property $G_{kj}(\mathbf{x}, \mathbf{y}) = G_{jk}(\mathbf{y}, \mathbf{x})$ and if $\mathbf{u}$ vanishes on the surface Σ and is a rigid-body motion on S the last integral on the right-hand side of (12) is zero. One thus obtains the single-layer integral representation

$$u_j(\mathbf{x}) = -\int_{S \cup \Sigma} f_k(\mathbf{y}) G_{jk}(\mathbf{x}, \mathbf{y}) dS(\mathbf{y}), \ \mathbf{x} \text{ in } \Omega. \tag{13}$$

By superposition the Cartesian components G_{jk} of any Green tensor $\mathbf{G}$ actually read

$$G_{jk}(\mathbf{x}, \mathbf{y}) = G_{kj}^\infty(\mathbf{x}, \mathbf{y}) + \Sigma_{jk}(\mathbf{x}, \mathbf{y}) \tag{14}$$

with velocity fields $\Sigma_{jk}(\mathbf{x}, \mathbf{y})\mathbf{e}_k$ smooth and bounded in the domain $\mathscr{D}$. Recalling (11), each component G_{jk} is thus weakly singular as $\mathbf{x}$ tend to $\mathbf{y}$ and (13) consequently also holds for $\mathbf{x}$ on S. Hence, the traction $\mathbf{f}$ obeys the Fredholm boundary-integral equation of the first kind

$$u_j(\mathbf{x}) = -\int_{S \cup \Sigma} f_k(\mathbf{y}) G_{jk}(\mathbf{x}, \mathbf{y}) dS(\mathbf{y}), \ \mathbf{x} \text{ on } S. \tag{15}$$

At this stage two different and possible choices occur for the Green tensor:

(i) First approach: one uses in (13) and (15) the free-space Green tensor $\mathbf{G}^\infty$ defined by (11) therefore putting so-called stokeslets of unknown density $\mathbf{f}$ on the entire surface $S \cup \Sigma$. This procedure appeals to a Green tensor available in closed

form and holds whatever the cavity shape. It however requires to obtain the traction **f** also on the entire surface Σ.

(ii) Second approach: one resorts to the Green tensor **G**^{c} which complies with the no-slip condition on the cavity boundary Σ i. e. such that its Cartesian components satisfy $G^c_{jk}(\mathbf{x}, \mathbf{y}) = 0$ for **x** on Σ. If **y** lies on Σ note that also $G^c_{jk}(\mathbf{x}, \mathbf{y}) = G^c_{kj}(\mathbf{y}, \mathbf{x}) = 0$ and the previous identities (13) and (15) thus become

$$u_j(\mathbf{x}) = - \int_S f_k(\mathbf{y}) G^c_{jk}(\mathbf{x}, \mathbf{y}) dS(\mathbf{y}), \quad \mathbf{x} \text{ in } \Omega \cup S. \tag{16}$$

The numerical implementation of (16) requires to determine the Green tensor **G**^{c} but solely involves the particle's surface S and thereby circumvents meshing the cavity boundary Σ which may become large.

3.3 Green tensor for a spherical cavity

The required Green tensor Cartesian components $G^c_{jk}(\mathbf{x}, \mathbf{y})$ for a spherical cavity with center O and radius R have been analytically obtained in Oseen (1927). Setting

$$\mathbf{y}' = \frac{R^2 \mathbf{y}}{|\mathbf{y}|^2}, \ \mathbf{r}' = \mathbf{x} - \mathbf{y}', \ r' = |\mathbf{r}'|, \ \mathbf{x}.\frac{\mathbf{y}'}{|\mathbf{y}'|} = |\mathbf{x}| \cos\theta, \tag{17}$$

his results for the regular Cartesian components $\Sigma_{jk} = G^\infty_{jk} - G^c_{jk}$ introduced by (14) may be cast into the following form

$$\Sigma_{jk}(\mathbf{x}, \mathbf{y}) = -\frac{R\delta_{jk}}{|\mathbf{y}|r'} - \left(\frac{R}{|\mathbf{y}|}\right)^3 \frac{[\mathbf{r}'.\mathbf{e}_j][\mathbf{r}'.\mathbf{e}_k]}{r'^3}$$
$$- \frac{|\mathbf{y}|^2 - R^2}{|\mathbf{y}|} \left\{ \frac{|\mathbf{x}|^2 - R^2}{2|\mathbf{y}|^2} \frac{\partial v_k}{\partial x_j} \right.$$
$$+ \frac{(\mathbf{y}'.\mathbf{e}_j)(\mathbf{y}'.\mathbf{e}_k)}{R^3 r'} [1 + 2\frac{\mathbf{y}'.\mathbf{r}'}{r'^2}]$$
$$\left. - \frac{R[(\mathbf{y}'.\mathbf{e}_j)(\mathbf{r}'.\mathbf{e}_k) + (\mathbf{y}'.\mathbf{e}_k)(\mathbf{r}'.\mathbf{e}_j)]}{|\mathbf{y}|^2 r'^3} \right\} \tag{18}$$

with δ_{jk} the Kronecker delta and $\mathbf{v} = v_k \mathbf{e}_k$ the vector

$$\mathbf{v} = \frac{R\mathbf{r}'}{r'^3} - \frac{2[\mathbf{r}'.\mathbf{y}']}{Rr'^3} \mathbf{y}'$$
$$+ \frac{3\{|\mathbf{x}| + [r' - |\mathbf{y}'|] \cos\theta\}}{R|\mathbf{x}||\mathbf{y}'|^2 \sin^2\theta} [R^2 \mathbf{x} - (\mathbf{x}.\mathbf{y}')\mathbf{y}]. \tag{19}$$

4 Migration in a gravity field and/or a rotating cavity

This section shows how to determine the rigid-body motion $(\mathbf{U}, \mathbf{W})$ of a particle induced by a gravity field **g** and/or a rotation $w_c \mathbf{e}$ of the spherical cavity by exploiting the results obtained in §3.

4.1 Incurred rigid-body migration

The flow $(\mathbf{u}, p)$ about the particle satisfies (3)-(5) and (7) together with, using the reciprocal identity (see Kim and Karrila (1991)), the basic identities

$$\int_{S \cup \Sigma} \mathbf{u}.\mathbf{f}^{(i)}_L dS = \int_{S \cup \Sigma} \mathbf{u}^{(i)}_L. \ \sigma.\mathbf{n} dS. \tag{20}$$

Recalling that

$$\mathbf{U}' = \mathbf{U} + w_c \mathbf{OO}' \wedge \mathbf{e}, \ \ \mathbf{W}' = \mathbf{W} - w_c \mathbf{e} \tag{21}$$

setting $\mathbf{U}' = U'_j \mathbf{e}_j, \mathbf{W}' = W'_j \mathbf{e}_j$ and also

$$A^{i,j}_L = A^{(i)}_L.\mathbf{e}_j, \ \ B^{i,j}_L = B^{(i)}_L.\mathbf{e}_j, \tag{22}$$

then easily makes it possible to cast (7) under the form

$$\mathbf{F}_h.\mathbf{e}_i = -[A^{i,j}_T U'_j + B^{i,j}_T W'_j] = (\rho - \rho_s)\mathscr{V} \mathbf{g}.\mathbf{e}_i, \tag{23}$$

$$\mathbf{T}_h.\mathbf{e}_i = -[A^{i,j}_R U'_j + B^{i,j}_R W'_j] = 0. \tag{24}$$

Injecting (21) in (23)-(24) finally gives

$$A^{i,j}_T U_j + B^{i,j}_T W_j = (\rho_s - \rho)\mathscr{V} \mathbf{g}.\mathbf{e}_i$$
$$- w_c [A^{i,j}_T (\mathbf{OO}' \wedge \mathbf{e}).\mathbf{e}_j - B^{i,j}_T \mathbf{e}.\mathbf{e}_j], \tag{25}$$

$$A^{i,j}_R U_j + B^{i,j}_R W_j =$$
$$- w_c [A^{i,j}_R (\mathbf{OO}' \wedge \mathbf{e}).\mathbf{e}_j - B^{i,j}_R \mathbf{e}.\mathbf{e}_j]. \tag{26}$$

As in Sellier and Pasol (2006) it is possible to prove that (25)-(26) has a real-valued, symmetric and positive-definite square matrix and therefore a unique solution $(\mathbf{U}, \mathbf{W})$ here obtained by solely

calculating the vectors $\mathbf{A}_L^{(i)}$ and $\mathbf{B}_L^{(i)}$ defined in (9). Let us denote by $(\mathbf{U}^0, \mathbf{W}^0)$ the solution for a motionless cavity $(w_c = 0)$. Inspecting (25)-(26) then readily shows that

$$\mathbf{U} = \mathbf{U}^0 + w_c \mathbf{e} \wedge \mathbf{OO'}, \quad \mathbf{W} = \mathbf{W}^0 + w_c \mathbf{e}. \qquad (27)$$

The relations (27) then describe the simple influence of the cavity rotation upon the sedimentation of the particule.

4.2 Disturbed velocity field in the cavity

Once $(\mathbf{U}, \mathbf{W})$ is known it is also possible, if needed, to calculate in the cavity the disturbed velocity field $\mathbf{u}_t = \mathbf{u} + w_c \mathbf{e} \wedge \mathbf{x}$ using on $S \cup \Sigma$ the boundary conditions (4)-(5) and in the liquid domain Ω the integral representations (13) or (16) for the Cartesian component $u_j = \mathbf{u}.\mathbf{e}_j$ with the surface traction $\mathbf{f} = \sigma.\mathbf{n}$. By superposition, this traction reads

$$\mathbf{f} = [U_i + w_c(\mathbf{OO'} \wedge \mathbf{e}).\mathbf{e}_i]\mathbf{f}_T^{(i)} + [W_i - w_c \mathbf{e}.\mathbf{e}_i]\mathbf{f}_R^{(i)}. \qquad (28)$$

5 Numerical strategy and benchmarks

As shown in the previous sections, one solely needs to compute the tractions $\mathbf{f}_T^{(i)}$ and $\mathbf{f}_R^{(i)}$ exerted on the particle's surface when it translates or rotates in a motionless cavity. In practice one needs to numerically invert the proposed Fredholm boundary-integral equations of the first kind (15) or (16) and also to implement the associated velocity integral representations (see §4.2). In this section we briefly describe how each integral equation is solved and also benchmark the proposed numerical method against accurate results available for a spherical particle.

5.1 Numerical implementation

There is a considerable literature dealing with the numerical treatment of boundary-integral equations and we refer for details the reader to classical textbooks such as C. A. Brebbia and Wrobel (1984); Beskos (1998); Bonnet (1999) and also in other fields to Gardano and Dabnichki (2006), F. Duddeck (2006) and Sanz, Solis, and Dominguez

(2007). In the present work we use the collocation method described in Sellier and Pasol (2006) for a quite different Green tensor. For the sake of conciseness we thus briefly introduce the technique but pay a special attention to the treatment of the regular part of the Green tensor given in (18). The particle's surface S is discretized using a N−node mesh made of 6−node isoparametric and curvilinear boundary elements. The associated quadratic shape functions and the adopted procedure to remove the weakly-singular contribution of the Oseen-Burgers tensor $\mathbf{G}^\infty$ by using local polar coordinates are detailed in Sellier (2007) and thus not reproduced here. When using (in our second approach; see §3.2) the Green tensor $\mathbf{G}^c$ of the spherical cavity one also needs to compute the regular components $\Sigma_{jk}(\mathbf{x}, \mathbf{y})$ for a pole $\mathbf{y}$ and a so-called field point $\mathbf{x}$ located on S. Unfortunately, (18) is not well-adapted for such a numerical implementation as $|\mathbf{y}|$ and/or $\sin\theta$ tend to zero. Introducing the quantities

$$\mathbf{y}' = \frac{R^2 \mathbf{y}}{|\mathbf{y}|^2}, \ \mathbf{t} = \frac{\mathbf{y}}{|\mathbf{y}|}, \ \mathbf{a} = \mathbf{x} - (\mathbf{x}.\mathbf{t})\mathbf{t}, \ h = \frac{|\mathbf{x} - \mathbf{y}'||\mathbf{y}|}{R}, \qquad (29)$$

and resorting to elementary manipulations too long to be reproduced here it has been found preferable to adopt the equivalent forms

$$\Sigma_{jk}(\mathbf{x}, \mathbf{y}) =$$
$$-\frac{\delta_{jk}}{h} - \frac{(\mathbf{x}.\mathbf{e}_j)(\mathbf{x}.\mathbf{e}_k)}{h^3} + \frac{(\mathbf{t}.\mathbf{e}_j)(\mathbf{t}.\mathbf{e}_k)}{h}\left[\frac{|\mathbf{x}|^2}{h^2} - 1\right]$$
$$-\left[\frac{2|\mathbf{y}|\mathbf{t}.\mathbf{x}}{h^3}\right](\mathbf{t}.\mathbf{e}_j)(\mathbf{t}.\mathbf{e}_k)$$
$$+|\mathbf{y}|\left[\frac{(\mathbf{t}.\mathbf{e}_j)(\mathbf{x}.\mathbf{e}_k) + (\mathbf{t}.\mathbf{e}_k)(\mathbf{x}.\mathbf{e}_j)}{h^3}\right]$$
$$-\frac{[|\mathbf{x}|^2 - R^2][|\mathbf{y}|^2 - R^2]}{2}\left\{\frac{\delta_{jk}}{R^3 h^3}\right.$$
$$-\frac{3}{R^2}\left[\frac{(\mathbf{h}.\mathbf{e}_j)(\mathbf{h}.\mathbf{e}_k)}{h^5}\right]$$
$$-2\frac{\mathbf{t}.\mathbf{e}_k}{R^2}\left[\frac{\mathbf{t}.\mathbf{e}_j}{h^3} - \frac{3(\mathbf{h}.\mathbf{e}_j)(\mathbf{h}.\mathbf{t})}{h^5}\right]$$
$$+\frac{3A}{R^4 h}\left[\delta_{jk} - (\mathbf{t}.\mathbf{e}_k)(\mathbf{t}.\mathbf{e}_j)\right]$$
$$+\frac{3\mathbf{a}.\mathbf{e}_k}{R}\left[-\frac{E}{R^3 h}\left\{\frac{|\mathbf{y}|\mathbf{h}.\mathbf{e}_j}{Rh^2} + \frac{2\mathbf{a}.\mathbf{e}_j}{|\mathbf{a}|^2}\right\}\right.$$

$$+ \frac{\mathbf{E}.\mathbf{e}_j}{R^4 h^2 [|\mathbf{x}| \pm (\mathbf{x}.\mathbf{t}))]} + \mathbf{a}.\mathbf{e}_j \left[\frac{(2R^2) \pm |\mathbf{y}||\mathbf{x}|]}{R^4 h^2 |\mathbf{a}|^2} \right] \right] \right\}$$

$$(30)$$

with real E and vector $\mathbf{E}$ defined as

$$E = \left\{ |\mathbf{x}| \pm \frac{2R^2 \mathbf{x}.\mathbf{t}}{R^2 + Rh \mp |\mathbf{x}||\mathbf{y}|} \right\} / \{ |\mathbf{x}| \pm \mathbf{x}.\mathbf{t} \}, \quad (31)$$

$$\mathbf{E} = \mp |\mathbf{y}|\mathbf{x} + \left[|\mathbf{y}||\mathbf{x}| \pm (1 \mp 2)R^2 \right] \mathbf{t}$$

$$\pm 2 \left[\frac{2R^2 |\mathbf{y}|\mathbf{x} + [R^3 h \mp R^2 |\mathbf{y}||\mathbf{x}|]\mathbf{t}}{R^2 + Rh \mp |\mathbf{y}||\mathbf{x}|} \right] \quad (32)$$

and the use of upperscripts or subscripts in (30)-(32) for $\mathbf{x}.\mathbf{t} \geq 0$ or $\mathbf{x}.\mathbf{t} < 0$, respectively. If $\mathbf{y} = \mathbf{0}$ we furthermore set $\mathbf{y} = \varepsilon \mathbf{e}_1$ with $\varepsilon = 10^{-12}$ in (30) which therefore admits a sense. It has been numerically checked that (18) and the proposed form (30)-(32) satisfy the announced symmetry property $\Sigma_{jk}(\mathbf{x},\mathbf{y}) = \Sigma_{kj}(\mathbf{y},\mathbf{x})$ for points $\mathbf{x}$ and $\mathbf{y}$ inside the spherical cavity. Finally, each discretized boundary-integral equation then results in a linear system which, having a fully-populated $3N \times 3N$ square matrix, is solved by LU factorization.

5.2 Benchmark tests for a spherical particle

As mentioned in the introduction and to the author's very best knowledge, only results for a spherical particle have been obtained so far. In this subsection we thus test the proposed approaches (use of the free-space Green tensor $\mathbf{G}^\infty$ or of the specific Green tensor $\mathbf{G}^c$) against the literature in two different cases:

(i) Case of a sphere at the center of the cavity

As noticed in Happel and Brenner (1973), the very specific case of a sphere with radius a translating at the velocity $\mathbf{e}_i$ and located at the center of the spherical cavity has been analytically treated by Cunningham (1910) and Williams (1915). In addition to the liquid velocity field those authors obtained the net force $-\mathbf{A}_T^{(i)}$ acting on the sphere which is, by symmetry, aligned with $\mathbf{e}_i$. More precisely, if $\beta = a/R$ one gets $\mathbf{A}_T^{(i)} = 6\pi\mu a c(\beta)\mathbf{e}_i$ with $c > 0$ and $c(0) = 1$ (usual case of the unbounded fluid given by (1)). For $a < R < \infty$ one has the exact relation (Happel and Brenner

(1973))

$$c(\beta) = \frac{1 - \beta^5}{1 - \frac{9\beta}{4} + \frac{5\beta^3}{2} - \frac{9\beta^5}{4} + \beta^6}, \quad \beta = a/R < 1.$$

$$(33)$$

We denote by c_s or c_c the computed value of c using the Green tensor $\mathbf{G}^\infty$ on $S \cup \Sigma$ (first approach) or the Green tensor $\mathbf{G}^c$ on S (second approach). In practice, we put 1058 collocation points on Σ for the first approach and use a $N - node$ mesh on the particle's surface. The quantities c_s, c_c and the associated relative errors $\Delta c_c = |c_c - c|/c$ and $\Delta c_s = |c_s - c|/c$ are displayed in Tab. 1 versus N for $R/a = 1.1, 2, 5$.

As N increases a nice convergence towards the analytical ratio c is observed for both approaches. Note however that for the small sphere-cavity gap R-a=0.1a the (second) approach appealing to the Green tensor $\mathbf{G}^c$ provides more accurate results.

(ii) Case of a sphere not located at the center of the cavity

As soon as the sphere is not located at the spherical cavity center there is no more available analytical result equivalent to (18). Several authors (see O'Neill and Majumdar (1970a,b); Jones (2008)) however provided numerical results by resorting to bipolar coordinates. For example, using this method Jones (2008) was recently able to accurately provide the friction coefficients for a sphere translating or rotating in the cavity. For further purposes (see §6) let us introduce such quantities for ellipsoidal particles with semi-axis (a_1, a_2, a_3), center O' such that $\mathbf{OO'} = d\mathbf{e}_3$ and inequality

$$(x_1/a_1)^2 + (x_2/a_2)^2 + ([x_3 - d]/a_3)^2 \leq 1. \quad (34)$$

The distance d obeys $0 \leq d < R - a_3$ and is also such that the entire ellipsoid lies within the cavity (therefore sometimes requiring $R - d - a_3$ to be large enough depending upon the value of (a_1, a_2)). For symmetry reasons, the net force $-\mathbf{A}_L^{(i)}$ and torque $-\mathbf{B}_L^{(i)}$ (recall (9)) then take the form (without summation over indices in (35))

$$\mathbf{A}_T^{(i)} = 6\pi\mu a_3 c_i \mathbf{e}_i, \quad \mathbf{B}_R^{(i)} = 8\pi\mu a_3^3 t_i \mathbf{e}_i, \quad (35)$$

Table 1: Computed quantities $c_s, \Delta c_s, c_c$ and Δc_c versus the number N of collocation points on the sphere's surface for $R/a = 1.1, 2, 5$. In calculating $(c_s, \Delta c_s)$ 1058 nodes have been used on Σ.

N	R/a	c_s	Δc_s	c_c	Δc_c
74	1.1	3258.137	1.00613	2097.155	0.29128
242	1.1	2124.983	0.30842	1949.547	0.01030
1058	1.1	1777.331	0.09436	1676.260	0.00353
exact	1.1	1624.089	0	1624.089	0
74	2.	7.223525	0.00968	7.218993	0.01030
242	2.	7.289179	0.00068	7.284937	0.00126
1058	2.	7.297493	0.00046	7.293273	0.00012
exact	2.	7.294118	0	7.294118	0
74	5.	1.749799	0.00344	1.749640	0.00353
242	5	1.755232	0.00035	1.755073	0.00044
1058	5.	1.755937	0.00005	1.755777	0.00004
exact	5.	1.755845	0	1.755845	0

$$\mathbf{B}_T^{(1)} = -8\pi\mu a_3^2 s_1 \mathbf{e}_2, \quad \mathbf{B}_T^{(2)} = 8\pi\mu a_3^2 s_2 \mathbf{e}_1,$$
$$\mathbf{B}_T^{(3)} = \mathbf{0}, \tag{36}$$

$$\mathbf{A}_R^{(1)} = 8\pi\mu a_3^2 s_2 \mathbf{e}_2, \quad \mathbf{A}_R^{(2)} = -8\pi\mu a_3^2 s_1 \mathbf{e}_1,$$
$$\mathbf{A}_R^{(3)} = \mathbf{0}, \tag{37}$$

where the dimensionless and so-called friction coefficients c_i, t_i, s_1 and s_2 depend upon $(a_1/a_3, a_2/a_3, d/a_3, R/a_3)$. For a sphere with radius a then $a_i = a$ and one furthermore gets $c_1 = c_2, t_1 = t_2$ and $s = s_2 = s_1$ therefore ending up with solely five friction coefficients c_1, c_3, t_1, t_3 and s also introduced and computed in Jones (2008). Comparisons with computations kindly provided on request by R. B. Jones for $R = 4a$ and two different normalized sphere-cavity gaps $\eta = (R - d - a)/a$ have been performed for both approaches. The results for the first approach employing the free-space Green tensor $\mathbf{G}^\infty$ and the entire surface $S \cup \Sigma$ are reported in Tab. 2. Because the sphere-cavity gap becomes small it has been required to use on the boundary Σ more collocations points than for the case of a sphere at the center of the cavity. Using 4098 nodes on Σ made it possible to gain a very good agreement with Jones results for $\eta = 0.5$ (medium gap) and $\eta = 0.1$ (small gap).

As revealed by Tab. 3, the second approach using the Green tensor $\mathbf{G}^c$ also permits one to obtain a nice convergence towards the values computed by Jones. It also turns out that this second approach yields more accurate results, especially for the small gap $\eta = 0.1$, than the first (usual) one which would actually require for a comparable accuracy to put more than 4098 collocation points on Σ for such a small gap and thus become prohibitive in terms of memory space and cpu time cost.

In summary, both approaches nicely recover for a spherical particle the accurate results previously obtained by other authors exploiting quite different and analytical procedures. Since it yields faster computations at a reasonable memory space price the (second) method appealing to the Green tensor $\mathbf{G}^c$ derived by Oseen (1927) for the spherical cavity is employed for all the numerical computations reported in §6.

6 Numerical results for non-spherical particles and discussion

Contrary to previous works, the advocated procedure also holds for non-spherical particles. This permits one to examine to which extent the net force $-\mathbf{A}_L^{(i)}$ and torque $-\mathbf{B}_L^{(i)}$ (recall (9)) and the incurred rigid-body motion $(\mathbf{U}, \mathbf{W})$ depend upon the particle's geometry and location inside the cavity. For such a purpose we consider ellipsoidal particles with uniform density $\rho_s \neq \rho$, center of volume O' with $\mathbf{OO'} = d\mathbf{e}_3$, semiaxes a_1, a_2, a_3 and inequality (34). For a motionless cavity (i. e. for $w_c = 0$) symmetries of the addressed con-

Table 2: Computed friction coefficients versus the number N of collocation points on S (with $N_1 = 74, N_2 = 242, N_3 = 1058$) for $R = 4a$ and two dimensionless sphere-cavity gaps η using the free-space Green tensor $\mathbf{G}^\infty$ (first approach) with 4098 collocation points on Σ. The results kindly provided by R. B. Jones are labelled J.

N	η	c_1	c_3	t_1	t_3	s
N_1	0.5	2.6330	4.6730	1.1640	1.0789	0.11870
N_2	0.5	2.6473	4.7107	1.1639	1.0755	0.11927
N_3	0.5	2.6488	4.7144	1.1639	1.0755	0.11938
J	0.5	2.6487	4.7131	1.1639	1.0755	0.11933
N_1	0.1	3.9016	15.552	1.6065	1.1960	0.20206
N_2	0.1	3.9273	18.886	1.6145	1.1939	0.19108
N_3	0.1	3.9159	18.832	1.6171	1.1945	0.18494
J	0.1	3.9121	18.674	1.6163	1.1945	0.18344

Table 3: Computed friction coefficients versus the number N of collocation points on S (with $N_1 = 74, N_2 = 242, N_3 = 1058$) for $R = 4a$ two dimensionless sphere-cavity gaps η using the Green tensor $\mathbf{G}^c$ (second approach). The results kindly provided by R. B. Jones are labelled J.

N	η	c_1	c_3	t_1	t_3	s
N_1	0.5	2.6327	4.6714	1.1639	1.0789	0.11861
N_2	0.5	2.6471	4.7090	1.1639	1.0755	0.11920
N_3	0.5	2.6486	4.7127	1.1639	1.0755	0.11932
J	0.5	2.6487	4.7131	1.1639	1.0755	0.11933
N_1	0.1	3.9009	15.413	1.6052	1.1960	0.20138
N_2	0.1	3.9237	18.636	1.6134	1.1938	0.19001
N_3	0.1	3.9121	18.711	1.6160	1.1945	0.18353
J	0.1	3.9121	18.674	1.6163	1.1945	0.18344

figuration show that the gravity-driven migration $(\mathbf{U}^0, \mathbf{W}^0)$ of the ellipsoidal particle with typical length scale a is such that

(i) If $\mathbf{g} = g\mathbf{e}_1$:

$$\mathbf{U}^0 = U'_s u_1 \mathbf{e}_1, \ \mathbf{W}^0 = aU'_s w_2 \mathbf{e}_2, \tag{38}$$

(ii) If $\mathbf{g} = g\mathbf{e}_2$:

$$\mathbf{U}^0 = U'_s u_2 \mathbf{e}_2, \ \mathbf{W}^0 = -aU'_s w_1 \mathbf{e}_1, \tag{39}$$

(iii) If $\mathbf{g} = g\mathbf{e}_3$:

$$\mathbf{U}^0 = U'_s u_3 \mathbf{e}_3, \ \mathbf{W}^0 = \mathbf{0} \tag{40}$$

with $U'_s = (\rho_s - \rho)a^2 g/\mu$ a typical settling velocity.

Let us first consider a sphere with radius a and two spheroids with typical length scale a, semi-axes $a_1 = t'a, a_2 = a_3 = ta$ and $t'/t = 1/2$ (oblate spheroid) or $t'/t = 3/2$ (prolate spheroid). We select (t, t') so that the sphere and each spheroid settle (without rotating) in an unbounded liquid at the same velocity $\mathbf{U}_s = 2(\rho_s - \rho)a^2\mathbf{g}/9$ as soon as $\mathbf{g} \wedge \mathbf{e}_1 = \mathbf{0}$. Note that those particles by contrast do not admit the same velocity if $\mathbf{g}$ is parallel to the axis of revolution $(O', \mathbf{e}_1)$. According to Happel and Brenner (1973) and setting $l = t'/t$, one arrives at $t = t(l)$ with

$$\frac{8}{3t^2} =$$
$$\frac{l^2}{l^2 - 1} + \frac{2l^3 - 3l}{(l^2 - 1)^{3/2}} \log(l + \sqrt{l^2 - 1}), \ l < 1,$$
$$\tag{41}$$

$$\frac{8}{3t^2} =$$
$$\frac{2l^2}{1 - l^2} + \frac{2(l - 2l^3)}{(1 - l^2)^{3/2}} \arctan(\frac{\sqrt{1 - l^2}}{l}), \ l > 1.$$
$$\tag{42}$$

The sphere with radius a has volume $\mathscr{V}_s$ and denoting by $\mathscr{V}$ the spheroid's volume it follows that $a_1 \sim 0.6296a, a_2 = a_3 \sim 1.2591a$ and $\mathscr{V}/\mathscr{V}_s \sim 0.9981$ for the oblate spheroid ($l = 1/2$) whilst $a_1 \sim 1.3384a, a_2 = a_3 \sim 0.8923a$ and $\mathscr{V}/\mathscr{V}_s \sim$

1.066 for the prolate one ($l = 3/2$). When a spheroid is located at the cavity center ($d = O$) it does not rotate and $u_2 = u_3$. For comparisons, the velocity u_2 is plotted in Fig. 2 versus the ratio $R/a \geq 1.5$ for each addressed spheroid. Those
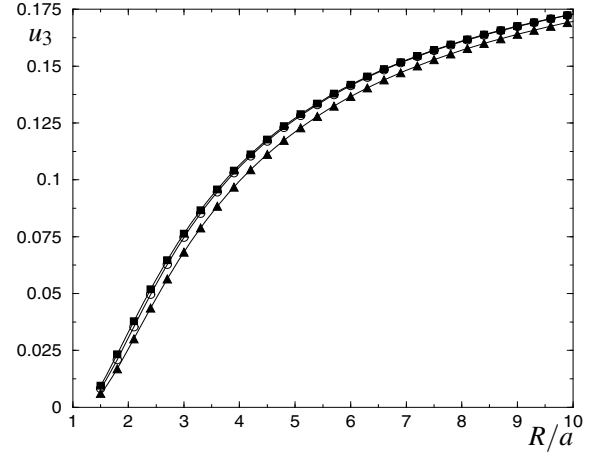

Figure 2: Normalized settling velocity $u_2 = u_3$ versus $R/a \geq 1.5$ for three equivalent (i. e. with identical settling velocities as $R/a \to \infty$ when $\mathbf{g} \wedge \mathbf{e}_1 = \mathbf{0}$) sphere (○), oblate spheroid (■) and prolate spheroid (▲) located at the center of the cavity.

results reveal that, for a particle located at the cavity center, the wall-particle interactions dramatically slow down each particle as the cavity radius decreases but are weakly shape-dependent. Moreover, the prolate spheroid is seen to adopt the smallest velocity for each prescribed ratio R/a whereas the oblate one experiences nearly the same velocity as the sphere.

However, the previous trends are likely to be modified for particles close to the cavity but not centered at its center. This issue is examined by computing the velocities u_2, u_3 and w_1 versus $R/a \geq 2$ for a given particle-wall gap equal to $0.5a$ (i. e. for $d = R - a_3 - 0.5a$). The results, displayed in Fig. 3, reveal that u_2, u_3 and w_1 this time deeply depend upon the particle's shape. The oblate or prolate spheroid rotates slower or faster than the equivalent sphere, respectively and each spheroid translates faster than the sphere except the prolate one when sedimenting normal to the cavity (u_3

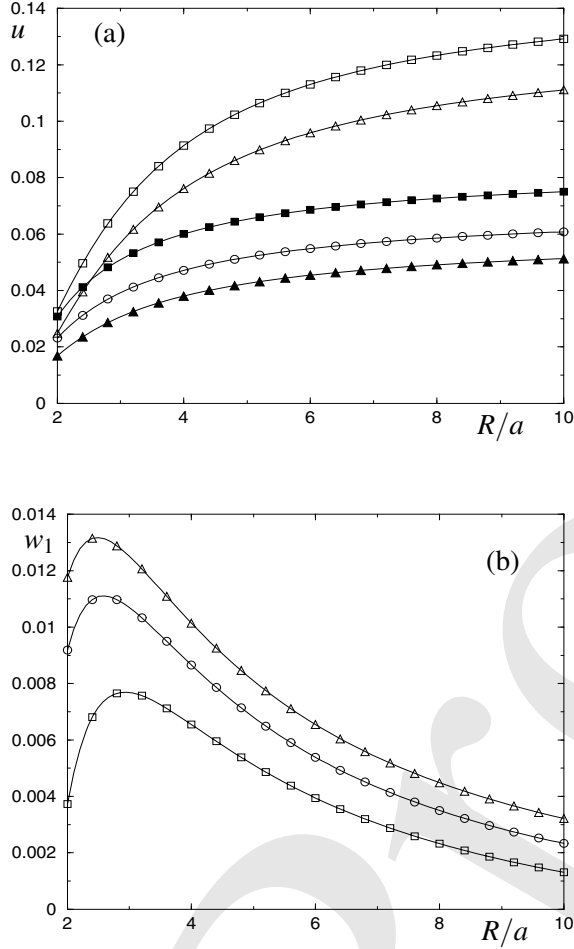component). The previous results clearly indicate

Figure 3: Normalized velocities u_2, u_3 and w_1 versus $R/a \geq 2$ for three equivalent sphere (circles with $u_2 = u_3$), oblate spheroid (squares) and prolate spheroid (triangles) not centered at the cavity center with $d = R - a_3 - 0.5a$. (a) Translational velocities u_2 (clear symbols) and u_3 (filled symbols). (b) Angular velocity w_1.

that the behaviour of a particle strongly depends upon its location inside the cavity. We further illustrate this key feature by changing the particle's location for a given cavity. For comparisons, those investigations have been achieved for two particles having the same volume and density ρ_s : a sphere with radius a and the non-spheroidal ellipsoid with inequation (34) and semi-axis $a_1 = 5a/3, a_2 = 0.6a$ and $a_3 = a$. As explained in §5.2, the relations (35)-(37) hold with $a = a_3$ and we

also use (38)-(40). The behaviour of each particle is therefore characterized by 13 dimensionless quantities c_i, t_i, u_i for $i = 1, 2, 3$ and also s_l, w_l for $l = 1, 2$ which solely depend upon the normalized parameters R/a and λ such that

$$R/a > 1 \quad \text{and} \quad 0 \leq \lambda = d/a < R/a - 1. \quad (43)$$

Such quantities have been computed for $R/a = 3$ and $\lambda \leq 1.9$ (i. e. up to a small particle-cavity gap of $0.1a$; a value at which the ellipsoid does not touch the cavity for $R = 3a$) by using 1058 or 1634 collocation points on the spherical or ellipsoidal particle, respectively. The results also take into account that $c_1 = c_2, t_1 = t_2, s_1 = s_2, u_1 = u_2$ and $w_1 = w_2$ for the sphere.

The computed velocities u_1, u_2, u_3, w_1 and w_2 are drawn versus λ in Fig. 4 where the sphere and the ellipsoid having the same volume adopt quite different settling velocities in presence of the gravity **g**. The ellipsoid rotates faster than the sphere if **g** is aligned with $\mathbf{e}_1$ at a positive angular velocity w_2 whereas it exhibits a more subtle rotation if **g** is aligned with $\mathbf{e}_2$: the angular velocity w_1 is positive or negative for $d < d_c$ or $d > d_c$, respectively and vanishes at the critical value $d_c \sim 1.5a$. Although each component u_i is seen in Fig. 4a to decrease, due to increasing wall-particle interactions, as $d = \lambda a$ increases the translational velocities of the two particles exhibit various trends. The ellipsoid translates faster or slower than the sphere if **g** is aligned with or normal to $\mathbf{e}_1$, respectively. Moreover, if $u_1 = u_2 > u_3$ for the sphere note that $u_3 - u_2$ may either be positive, zero or negative depending upon d. In other words, there exist a critical location $d_l \sim 1.27a$ at which the ellipsoid adopts the same translational velocity for $\mathbf{g} = g\mathbf{e}_2$ and $\mathbf{g} = g\mathbf{e}_3$. This is clearly not the case for the sphere. How the velocity of each considered particle is affected by a rotation of the cavity at the velocity $w_c\mathbf{e}$ is given by (27). Whereas one has only to add $w_c\mathbf{e}$ to the angular velocity $\mathbf{W}^0$ (whatever the particle shape and position) the case of the translational velocity is more tricky and it is possible to tune the rotation of the cavity to vanish the velocity **U**. For example, if $\mathbf{g} = g\mathbf{e}_1$ and $\rho_s \neq \rho$ one obtains $\mathbf{U} = (\rho_s - \rho)a^2gu/\mu\mathbf{e}_1$ when
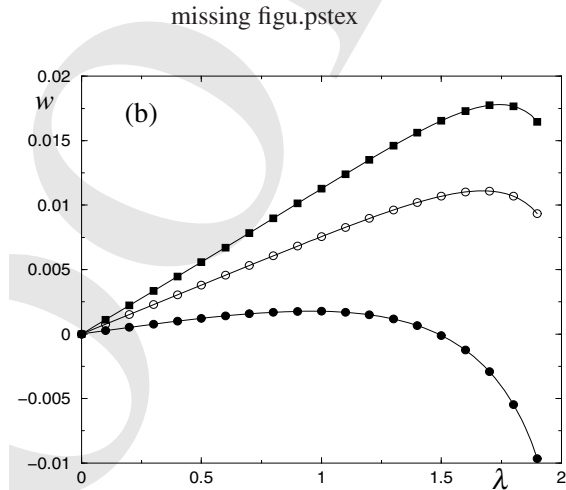
missing figu.pstex

Figure 4: Normalized velocities for the sphere (clear symbols) and the ellipsoid (filled symbols). (a) Translational velocities u_1 (circles), u_2 (squares) and u_3 (triangles). (b) Angular velocities w_1 (circles) and w_2 (squares).

the cavity rotates at the velocity $w_c \mathbf{e}_2$ with

$$u = u_1 + \lambda A w_c, \quad A = \mu/[(\rho_s - \rho)ag] \neq 0 \qquad (44)$$

and therefore for a given location λ the particle does not translate when the cavity rotates at the critical angular velocity $-u_1 \mathbf{e}_2/[\lambda A]$.

The coefficients c_i, t_i, s_1 and s_2 are plotted in Fig. 5 and Fig. 6. Each coefficient is seen to weakly and strongly vary for $d = \lambda a$ smaller or greater than unity, respectively with wall-particle interactions significantly acting for a sufficiently small wall-particle gap and increasing the magnitude of each coefficient. The ellipsoid and the sphere exhibit either very close behaviours for c_1, c_3, t_1 or quite different behaviours for the other coefficients. One should also note that s_2 for the ellipsoid is either positive for $d < d_c$, zero for $d = d_c \sim 1.488a$ or negative $d > d_c$.

7 Conclusions

Two possible boundary-integral appoaches have been proposed and implemented to investigate the rigid-body and/or gravity-driven motion of a solid and arbitrarily-shaped particle in a spherical cavity. The first method spreads free-space Stokeslets
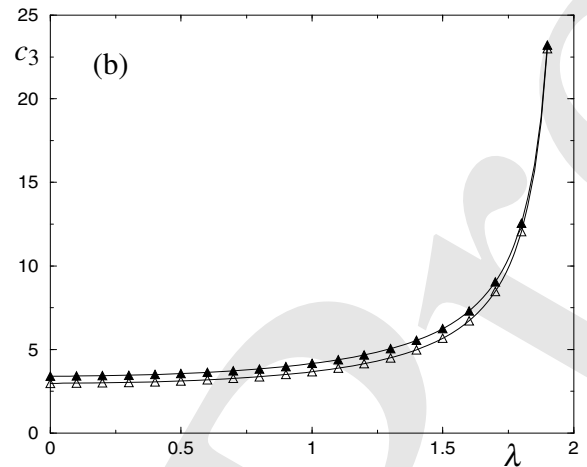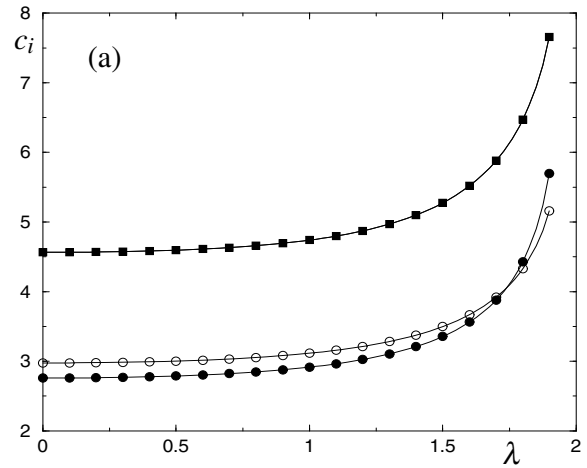

Figure 5: Normalized coefficients c_i for the sphere (clear symbols) and the ellipsoid (filled symbols). (a) Coefficients c_1 (circles) and c_2 (squares). (b) Coefficients c_3 (triangles).

on both the cavity and the particle surface. It is by essence not restricted to a spherical cavity but requires to put a great deal of nodes on a cavity of medium or large size to ascertain a sufficient accuracy. The second method appeals to a specific Green tensor obtained in Oseen (1927) for a spherical boundary, i. e is not valid for non-spherical cavities, but solely requires to mesh the particle surface and yields at a quite reasonable cpu time cost very accurate results even for a large spherical cavity. The computations, performed with the second approach and for spheroidal or ellipsoidal particles, show that the net hydrody-
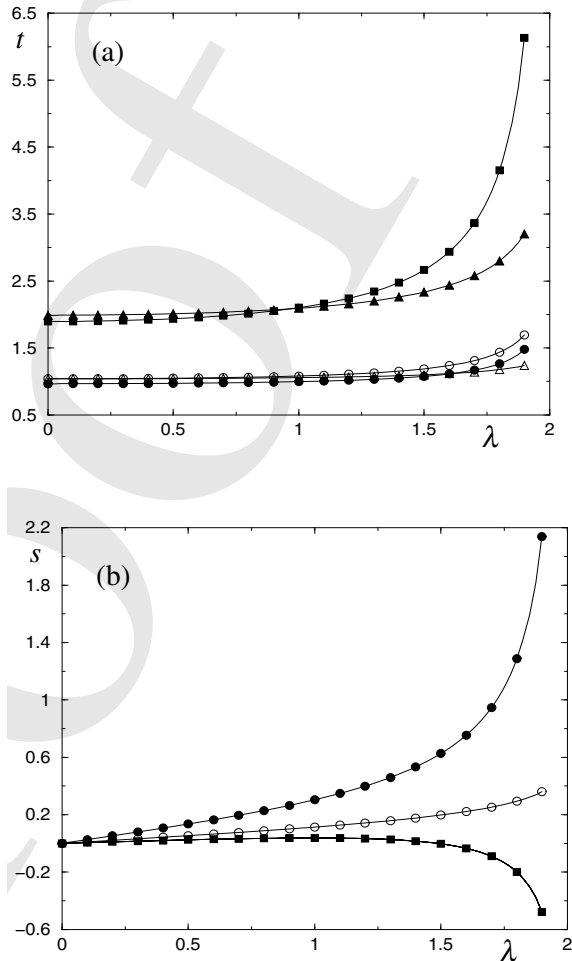
Figure 6: Normalized coefficients t_i and s_l for the sphere (clear symbols) and the ellipsoid (filled symbols). (a) Coefficients t_1 (circles), t_2 (squares) and t_3 (triangles). (b) Coefficients s_1 (circles) and s_2 (squares).

namic force and torque experienced by a particle together with its settling velocity deeply depend upon both the particle location inside the cavity and the particle shape. So-called 'equivalent' spheroid (which have identical settling velocities for a specific gravity direction in an unbounded fluid) are for instance seen to adopt slighltly different gravity-driven motion when inside and not at the center of a spherical cavity whilst a sphere and an ellipsoid of identical volume clearly exhibit different settling translation and rotations.

As explained in the introduction, this work makes it possible to examine the sedimentation of a dilute suspension by neglecting particule-particle interactions. This latter approximation of course breaks down for non-dilute suspensions for which close particules strongly interact. The analysis of such circumstances where both particle-particle and particle-boundary interactions play a role requires to extend the present theory to the general case of a $N - particle$ cluster in a spherical cavity. Such a work, however non trivial and therefore postponed to a further investigation, might be adequately handled for a large number of interacting particles by employing the fast multipole method proposed by P. B. Wang and Z. H. Yao (2005) and P. B. Wang and Z. H. Yao and T. Lei (2006).

References

Beskos, D. E. (1998): *Introduction to Boundary Element Methods.* Elsevier Science Publishers.

Bonnet, M. (1999): *Boundary Integral Equation Methods for Solids and Fluids.* John Wiley & Sons Ltd.

Brenner, H. (1961): The slow motion of a sphere through a viscous fluid towards a plane surface. *Chem. Engng Sci.*, vol. 16, pp. 242–251.

C. A. Brebbia, J. C. T.; Wrobel, L. C. (1984): *Boundary Element Techniques.* Springer-Verlag, Theory and Applications in Engineering, Berlin Heidelberg New York Tokyo.

Chaoui, M.; Feuillebois, F. (2003): Creeping flow around a sphere in shear flow close to a wall. *Q. J. Mech. Appl. Math.*, vol. 56, pp. 381–410.

Cichocki, B.; Jones, R. B. (1998): Image representation of a spherical particle near a hard wall. *Physica A*, vol. 258, pp. 273–302.

Cichocki, B.; Jones, R. B.; Kutteh, R.; Wajnryb, E. (2000): Friction and mobility for colloidal spheres in Stokes flow near a boundary. *J. Chem. Phys.*, vol. 112, no. 5, pp. 2548–2561.

Cunningham, E. (1910):   On the velocity of steady fall os spherical particles through fluid medium. *Proc. Roy. Soc*, vol. A, pp. 357–365.

Dean, W. R.; O'Neill, M. E. (1963):   A slow motion of viscous liquid caused by the rotation of a solid sphere. *Mathematika*, vol. 10, pp. 13–24.

F. Duddeck (2006):   An Alternative Approach to Boundary Element Methods via the Fourier Transform. *CMES: Computer Modeling in Engineering and Science*, vol. 15, no. 1, pp. 1–14.

Ganatos, P.; Peffer, R.; Weibaum, S. (1980a): A strong interaction therory for the creeping motion of a sphere between plane parallel boundaries. 1. Perpendicular motion. *J. Fluid Mech*, vol. 9, pp. 739–753.

Ganatos, P.; Peffer, R.; Weibaum, S. (1980b): A strong interaction therory for the creeping motion of a sphere between plane parallel boundaries. 1. Parallel motion. *J. Fluid Mech*, vol. 9, pp. 755–783.

Gardano, P.; Dabnichki, P. (2006):   Application of Boundary Element Method to Modelling of Added Mass and Its Effect on Hydrodynamic Forces. *CMES: Computer Modeling in Engineering and Science*, vol. 15, no. 2, pp. 87–98.

Goldman, A. J.; Cox, R. G.; Brenner, H. (1967a): Slow viscous motion of a sphere parallel to a plane wall. I. Motion through a quiescent fluid. *Chem. Engng Sci.*, vol. 22, pp. 637–651.

Goldman, A. J.; Cox, R. G.; Brenner, H. (1967b): Slow viscous motion of a sphere parallel to a plane wall. II. Couette flow. *Chem. Engng Sci.*, vol. 12, pp. 653–660.

Happel, J.; Brenner, H. (1973):   *Low Reynolds number hydrodynamics*. Martinus Nijhoff.

Hsu, R.; Ganatos, P. (1989):   The motion of a rigid body in viscous fluid bounded by a plane wall. *J. Fluid Mech*, vol. 207, pp. 29–72.

Hsu, R.; Ganatos, P. (1994):   Gravitational and zero-drag motion of a spheroid adjacent to an inclined plane at low Reynolds number. *J. Fluid Mech*, vol. 268, pp. 267–292.

Jeffery, G. B. (1915): On the steady rotation of a solid of revolution in a viscous fluid. *Proc. Lond. Math. Soc. (Series 2)*, vol. 14, pp. 327–338.

Jones, R. B. (2004):   Spherical particle in Poiseuille flow between planar walls. *Journal of Chemical Physics*, vol. 121, pp. 483–500.

Jones, R. B. (2008):   Dynamics of a colloid in a spherical cavity. *To appear in Methods of creeping flows. Editors: F.Feuillebois and & A. Sellier.*

Kim, S.; Karrila, S. J. (1991):   *Microhydrodynamics: Principles and Selected Applications*. Butterworth.

O'Neill, M. E. (1964): A slow motion of viscous liquid caused by a slowly moving solid sphere. *Mathematika*, vol. 11, pp. 67–74.

O'Neill, M. E. (1967): A slow motion of viscous liquid caused by a slowly moving solid sphere: an addendum. *Mathematika*, vol. 14, pp. 170–172.

O'Neill, M. E.; Majumdar, S. R. (1970): Asymmetrical slow viscous fluid motions caused by the translation or rotation of two spheres. Part I: the determination of exact solutions for any values of the ratio of radii and separation parameters. *J. Appl. Math. Phys.*, vol. 21, pp. 164–179.

O'Neill, M. E.; Majumdar, S. R. (1970): Asymmetrical slow viscous fluid motions caused by the translation or rotation of two spheres. Part II: asymptotic forms of the solutions when the minimum clearance between the spheres apporaches zero. *J. Appl. Math. Phys.*, vol. 21, pp. 180–187.

O'Neill, M. E.; Stewartson, K. (1967): On the slow motion of a sphere parallel to a nearby plane wall. *J. Fluid Mech.*, vol. 27, pp. 705–724.

Oseen, C. W. (1927):   *Neure Methoden und Ergebnisse in der Hydrodynamik*. Akademische Verlagsgesellschat M. B. H.

P. B. Wang and Z. H. Yao (2005): A New Fast Multipole boundary Element Method for large sacle analysis of mechanical properties in 3D

particle-reinforced composites. *CMES: Computer Modeling in Engineering and Science*, vol. 7, no. 1, pp. 85–96.

P. B. Wang and Z. H. Yao and T. Lei (2006): Analysis of solid with numerous microcracks using the Fast Multipole DBEM. *CMC: Computers, Materials, & Continua*, vol. 3, no. 2, pp. 65–76.

Pasol, L.; Chaoui, M.; Yahiaoui, S.; Feuillebois, F. (2005): Analytical solutions for a spherical particle near a wall in axisymmetrical polynomial creeping flows. *Phys. Fluids 17*, vol. 17, pp. 073602.1–073602.13.

Pasol, L.; Sellier, A. (2006): Gravitational motion of a two-particle cluster between two parallel plane walls. *Comptes Rendus Mécanique*, vol. 334, pp. 105–110.

Pasol, L.; Sellier, A.; Feuillebois, F. (2006): A sphere in a second degree polynomial creeping flow parallel to a wall. *Q. J. Mech. Appl. Math*, vol. 59, pp. 587–614.

Pozrikidis, C. (1992): *Boundary integral and singularity methods for linearized viscous flow.* Cambridge University Press.

Sanz, J.; Solis, M.; Dominguez, J. (2007): Hypersingular BEM for Piezoelectric Solids: Formulation and Applications for Fracture Mechanics. *CMES: Computer Modeling in Engineering and Science*, vol. 17, no. 3, pp. 215–230.

Sellier, A. (2007): Slow viscous migration of a conducting solid particle under the action of uniform ambient electric and magnetic fields. *CMES: Computer Modeling in Engineering and Science*, vol. 21, no. 2, pp. 105–132.

Sellier, A.; Pasol, L. (2006): Sedimentation of a Solid Particle Immersed in a Fluid Film. *CMES: Computer Modeling in Engineering and Science*, vol. 16, no. 3, pp. 187–196.

Staben, M. E.; Zinchenko, A. Z.; Davis, R. H. (2003): Motion of a particle between two parallel plane walls in low-Reynolds-number Poiseuille flow. *Physics of Fluids*, vol. 15, pp. 1711–1733.

Stimson, M.; Jeffery, G. B. (1926): The motion of two spheres in a viscous Fluid. *Proc. Roy. Soc.*, vol. A 111, pp. 110–121.

Williams, E. (1915): On the motion of a sphere in a viscous fluid. *Phil. Mag. 6th Serie*, vol. 29, pp. 526–555.